International Journal of Nanomedicine

Dovepress
open access to scientific and medical research

Open Access Full Text Article

ORIGINAL RESEARCH

Photothermal treatment of liver cancer with albumin-conjugated gold nanoparticles initiates Golgi Apparatus–ER dysfunction and caspase-3 apoptotic pathway activation by selective targeting of Gp60 receptor

This article was published in the following Dove Press journal:
International Journal of Nanomedicine
26 August 2015
Number of times this article has been viewed

Lucian Mocan[1,2]
Cristian Matea[1]
Flaviu A Tabaran[3]
Ofelia Mosteanu[1,4]
Teodora Pop[1,4]
Teodora Mocan[1,5]
Cornel Iancu[1,2]

[1]Nanomedicine Department, Regional Institute of Gastroenterology and Hepatology "Octavian Fodor", [2]Department of Surgery, University of Medicine and Pharmacy, "Iuliu Hatieganu", [3]Department of Pathology, Faculty of Veterinary Medicine, University of Agricultural Sciences and Veterinary Medicine, [4]Department of Gastroenterology, [5]Department of Physiology, University of Medicine and Pharmacy, "Iuliu Hatieganu", Croitorilor, Cluj-Napoca, Romania

Correspondence: Teodora Mocan; Cornel Iancu
Nanomedicine Department, Regional Institute of Gastroenterology and Hepatology 'Octavian Fodor', Croitorilor Street 19-21, Cluj Napoca, 400162, Romania
Tel +40 264 439 696
Fax +40 264 439 696
Email teodora.mocan@umfcluj.ro; cornel.iancu@umfcluj.ro

Abstract: We present a method of enhanced laser thermal ablation of HepG2 cells based on a simple gold nanoparticle (GNP) carrier system such as serum albumin (Alb), and demonstrate its selective therapeutic efficacy compared with normal hepatocyte cells. HepG2 or hepatocytes were treated with Alb-GNPs at various concentrations and various incubation times, and further irradiated using a 2 W, 808 nm laser. Darkfield microscopy and immunochemical staining was used to demonstrate the selective internalization of Alb-GNPs inside the HepG2 cells via Gp60 receptors targeting. The postirradiation apoptotic rate of HepG2 cells treated with Alb-GNPs ranged from 25.8% (for 5 μg/mL) to 48.2% (for 50 μg/mL) at 60 seconds, while at 30 minutes the necrotic rate increased from 35.7% (5 μg/mL) to 52.3% (50 μg/mL), *P*-value <0.001. Significantly lower necrotic rates were obtained when human hepatocytes were treated with Alb-GNPs in a similar manner. We also showed by means of immunocytochemistry that photothermal treatment of Alb-conjugated GNPs in liver cancer initiates Golgi apparatus–endoplasmic reticulum dysfunction with consequent caspase-3 apoptotic pathway activation and cellular apoptosis. The presented results may become a new method of treating cancer cells by selective therapeutic vectors using nanolocalized thermal ablation by laser heating.

Keywords: liver cancer, gold nanoparticles, HepG2 cells, functionalization, laser irradiation, albumin

Introduction

Hepatocellular carcinoma (HC), a common malignancy of the liver, represents a leading cause of cancer-related mortality.[1] Surgical resection of the tumor is the only accepted treatment, with curative intent being feasible in only 10%–30% of patients. Since chemotherapy and radiotherapy have produced modest results in HC treatment, new methods of therapy would bring about a better outcome.[2]

Most data suggest that nanotechnologies hold great hopes for the development of new cancer treatments.[3]

The ability of light-heat conversion in gold nanoparticles (GNPs) following near-infrared (NIR) laser radiation provides an opportunity to create novel nanoparticle-based therapies with high performance and efficacy in selective thermal ablation of cancer at a molecular level.[4–8]

Cancer nanotechnology, an interdisciplinary research domain, has already brought to light promising results in cancer diagnosis and treatment.[9] The first GNP therapy to

submit your manuscript | www.dovepress.com
Dovepress
http://dx.doi.org/10.2147/IJN.S86495

have reached early-phase clinical trials is CYT-6091, 27-nm citrate-coated GNPs bound with thiolated polyethylene glycol and tumor necrosis factor-α.[10] Intratumor-administered GNPs combined with laser irradiation proved to be efficient in the treatment of HC on animal models.[11] The holy grail in the treatment of HC is the development of selective therapies directed only at tumor cells inside liver parenchyma with no side effects on surrounding, healthy tissue.[10]

Various studies have proved that highly proliferative HC cells exhibit high intracellular albumin (Alb) levels. The reports have demonstrated the liver cancer cells' overexpression of specific human serum Alb receptors and their ability to internalize large amounts of Alb through the mechanism of caveolae-mediated endocytosis. The resulting amino acids are further used for the synthesis of various substrates needed for tumor growth.[12,13] Considering all these aspects of liver cancer metabolism, we report here a construct of an Alb-GNP bionanosystem for selective targeting of albondin (Gp60) receptors and laser-mediated necrosis of liver cancer cells with minimal harmful effects on normal cells. To our knowledge, this is the first demonstration of selective targeting via Gp60 receptors (located on the membrane of malignant liver cancer cells) using a conjugate of Alb and GNPs.

Methods

Gold nanoparticles functionalization

Bovine serum Alb (BSA) (≥98%), trisodium citrate (≥99%), $HAuCl_4$ (≥99.9%), DL-dithiotreitol (≥99%), and ammonium bicarbonate were purchased from Sigma-Aldrich™ (Darmstadt, Germany) and used without further purification.

In order to obtain citrate-capped GNPs, a modified Turkevich method was employed. Briefly, 24 mg $HAuCl_4$ was dissolved in 50 mL H_2O bidistilled and heated to 100°C. To this, a 5 mL trisodium citrate (4 mg/mL) solution was rapidly injected under vigorous stirring. The solution was kept under reflux for 2 hours and vigorous stirring; during this process, the color turned dark red. For coupling the Alb on the surface of the citrate-capped GNPs, the Alb was subjected to a reduction step using Cleland's reagent. Thus, 1 mL DTT 110 mM (pH =8.5) was added to a 10 mL Alb (1 mg/mL) aqueous solution and kept under stirring at 37°C for 45 minutes. Afterward, 3 mL of the citrate-capped GNPs obtained in the previous step were added to the Alb solution, and the pH was adjusted to 7. The reaction was allowed to continue for 1 hour at room temperature. The resulting Alb-GNP solution was subjected to a centrifugation step (16,000 rpm/30 minutes), and the resulting pellet was collected and re-dispersed in bidistilled water. The resulting Alb-GNP solution showed good stability over several weeks at room temperature.

UV-Vis spectroscopy was carried out using a Shimadzu UV-1800 spectrophotometer (Shimadzu Corporation, Kyoto, Japan). The spectras of Alb solution, citrate-capped GNPs, and Alb-functionalized GNPs were recorded from 800 to 200 nm with a spectral resolution of 0.5 nm. All recorded spectras were normalized using the OriginLab Software® 7.0 (OriginLab Corporation, Northampton, MA, USA).

Dynamic light scattering measurements were performed at a 90° scattering angle at 37°C by means of a Zetasizer Nano S90 intrument (Malvern Instruments, Westborough, UK).

Universal attenuated total reflectance Fourier transform infrared spectroscopy (ATR-FT-IR) was performed using a Perkin-Elmer Spectrum Two® instrument (Perkin-Elmer, Waltham, MA, USA) with a universal ATR single reflection diamond. Baseline corrections and spectra processing were done using the instruments Spectrum 10™ software (Perkin-Elmer).

Atomic force microscopy (AFM) measurements were carried out on a Workshop TT-AFM® (AFM Workshop, CA, USA) in vibrating mode using ACTA-SS cantilevers (AppNano, CA, USA). Samples were deposited on a mica substrate using a KLM® SCC spin coater (Schaefer Technologie GMBH, Langen, Germany). The recorded data were processed with the aid of Gwyddion® 2.36 software. Nanoparticle concentrations in solutions were calculated using the following formula: $C=A_{450}/\varepsilon_{450}$, where C is the particle concentration in mol/L, A is the absorption at 450 nm for a standard path length l of 1 cm, and ε was 3.24E+08.

Cell culture

HepG2 and HepB5 cells purchased from the European Collection of Cell Cultures were cultured in Minimum Essential Medium with 10% fetal bovine serum at 37°C in a humidified 5% CO_2 atmosphere using 25 cm^3 plastic tissue culture flasks (Corning Incorporated, Corning, NY, USA). Cells were in the logarithmic growth phase by routine passage every 2–3 days and split when reaching confluence. No ethics statement was required from the institutional review board for the use of these cell lines.

Microscopy analysis of cells

For the microscopy analysis, we used Lab-Tek Chamber Slide for in situ observation of the glass adherent cells (the walls were removed, and the media/GNP solution

was discharged). Thus, no cell transfer was needed prior to visualization/staining. All microscopic analyses were performed using a high-performance FSX-100 Olympus Microscope (Olympus Corporation, Tokyo, Japan). Phase-contrast and multi-excitation filter (R, B, G) fluorescence detection modes were used.

Laser treatment

The Alb-GNPs treated cells (5, 10, and 50 μg/mL, respectively) were next irradiated for 2 minutes, using an 808 nm laser, 2 W/cm^2 power. The medium was removed before irradiation, and the vertical position was assured for the laser diode (2 cm above the adherent cell layer). To provide uniformity of laser excitation regardless of the surface of the seeding well designed for various analysis techniques (4-well chamber, or 96-well plates), multiple irradiation spots were used for samples seeded in 4-well chambers (further analyzed by means of microscopy or flow cytometry techniques).

Annexin V-Cy3 Apoptosis Detection Assay

Apoptotic cells suggested by translocation of phosphatidylserine (PS) groups on the outer leaflet of the cell membrane were detected using Annexin-V Cy3 Apoptosis Detection Assay (BioVision, Inc, Milpitas, CA, USA) in accordance with manufacturer protocol. Cells were seeded into a 4-chamber glass slide (Millipore, Billerica, MA, USA). Briefly, immediately after exposure and irradiation, cells were incubated with Annexin-V Cy3 (5 minutes, dark), followed by microscopic examination using a rhodamine filter. Analysis of the samples was performed using fluorescence microscopy combined with flow cytometry.

Golgi Apparatus, Endoplasmic Reticulum, and Nucleus Detection Assay

Multiple organelle staining was performed using an Organelle-ID RGB III Assay kit (Enzo Life Sciences, Farmingdale, NY, USA), which allows selective endoplasmic reticulum (ER), golgi apparatus (GA), and nucleus (N) staining, in accordance with manufacturer suggestions. Both HepG2 and HepB5 cells were washed with 100 μL assay solution and further treated with Organelle-ID RGB Reagent III solution (100 μL/chamber, 4°C, dark room). After 30 minutes of incubation, a second washing step was performed (3× ice-cold medium), followed by fresh ice-cold medium incubation (37°C, 30 minutes). Next, cells were rinsed with a 100 μL, 1X assay solution. After the removal of buffer excess, fixation (formaldehyde 10%, 5 minutes) and washing (deionized water) were performed. Next, the medium chamber was detached from the slide, and the coverslip was placed and mounted (Water-based Mountant, Magnacol Ltd., Powys, UK). The slide was further analyzed using microscopy techniques. To detect the distinct fluorescent emissions signals, the following standard filter sets were used: FITC (GA), DAPI (N), and Texas Red (ER), respectively.

Analysis of cellular viability following Alb-GNPs mediated treatment

Red fluorescence, an indicator of necrotic cells stain with Annexin-V Cy3 (red, dead cells), was depicted using a FACSCalibur flow cytometer (Becton Dickinson, San Jose, CA, USA) (FL3 channel). All parameters intended for analysis were collected at low speed, in logarithmic mode (~15 μL/min), in order to maintain the counting level under 1,000 events/s. Population density was estimated using CellQuest software program.

Staining of GP60 receptors

Following treatment as described, cells were fixed with 3%–4% paraformaldehyde in phosphate-buffered saline (PBS) for 15 minutes at room temperature and ice-cold acetone for 7 minutes, respectively, and subsequently permeabilized with digitonin 0.2% in PBS for 10 minutes. Nonspecific binding of the antibodies was blocked in PBS containing 10% goat serum and 0.3 M glycine. After 30 minutes of incubation, the cells were further incubated with an anti-Alb receptor antibody (Abcam, Cambridge, UK) diluted to 1:50 in PBS at 4°C for 1 hour. Next, the cells were washed and then reacted with a Cy3 secondary antibody diluted to 1:1,000 at room temperature in the dark for 1 hour for detection. At the end, the cells were washed with PBS three times for 5 minutes in the dark.

In vitro augmented-dark-field light microscopy imaging of nanoparticle interaction with HepG2 cells

To assess the intracellular distribution in tumor cells, a CytoViva150 Ultrahigh Resolution Imaging System (CytoViva, Auburn, AL, USA) attached to an Olympus BX-43 microscope was used. Images were collected with a DAGE-MTI XL16 digital camera (DAGE-MTI, Michigan City, IN, USA) as 1,600×1,200 pixel/8 bit and processed with Exponent 7 Software. The CytoViva enhanced dark field-based illumination system, due to the high signal-to-noise, allows the direct intracellular visualization of nanoscale sample elements such as GNPs.

ImageJ analysis

For the quantitative analysis of ER and GA morphologic changes in HepG2 cells following Alb-GNPs mediated treatment, fluorescence quantification was done using ImageJ (National Institutes of Health, New York, NY, USA) software by measuring the stained area on a similar number of cells as previously described. Mean values correspond to signal intensity of ER or GA after subtraction of the nuclei fluorescence and normalization with the respective cellular area. Values are expressed as the percentage of the intensity of GA and ER fluorescence in control cells.[14]

Statistical analysis

All the presented data were expressed as median (range). Continuous enzyme-linked immunosorbent assay data were compared with control levels to obtain the percentage level for each group. The Kolmogorov–Smirnov test was chosen because of the non-normality of the data. Data comparisons for the same concentration between two groups were obtained using the Wilcoxon test. For all tests, an alpha error level of <0.05 was chosen. Statistical packages SPSS 17.0 (Chicago, IL, USA) as well as the Excel Application of Microsoft Office platform were used for data analyses.

Results

Functionalization of GNPs with Alb

The obtained Alb-stabilized GNPs were subjected to UV-Vis, dynamic light scattering (DLS), ATR-FT-IR, and AFM measurements.

UV-Vis spectroscopy measurements in the range of 250–800 nm revealed a surface plasmon resonance (SPR) peak at 521 nm for the citrate-capped GNPs.[15] Meanwhile, in the case of Alb-GNP, the SPR peak underwent a bathochromic shift of 7 nm (Alb-GNP λ_{max}=528 nm) (Figure 1A).[16]

In order to confirm the successful attachment of Alb on the GNP surface, ATR-FT-IR spectroscopy measurements were undertaken. Figure 1B depicts the FT-IR spectra of Alb-GNP and GNP. For the Alb-GNP sample, the two characteristic bands of BSA can be observed at 1,656 and 1,546 cm^{-1} attributable to the amide I and amide II, respectively. The band at 1,656 cm^{-1} is attributable to C=O stretching from the Alb, while the band at 1,546 cm^{-1} is a coupling of C–N stretching and N–H bending modes in the protein.[17] In the case of citrate-capped GNPs, the bands corresponding to the symmetric and antisymmetric stretching of COO^- of the citrate ions can be observed at 1,397 and

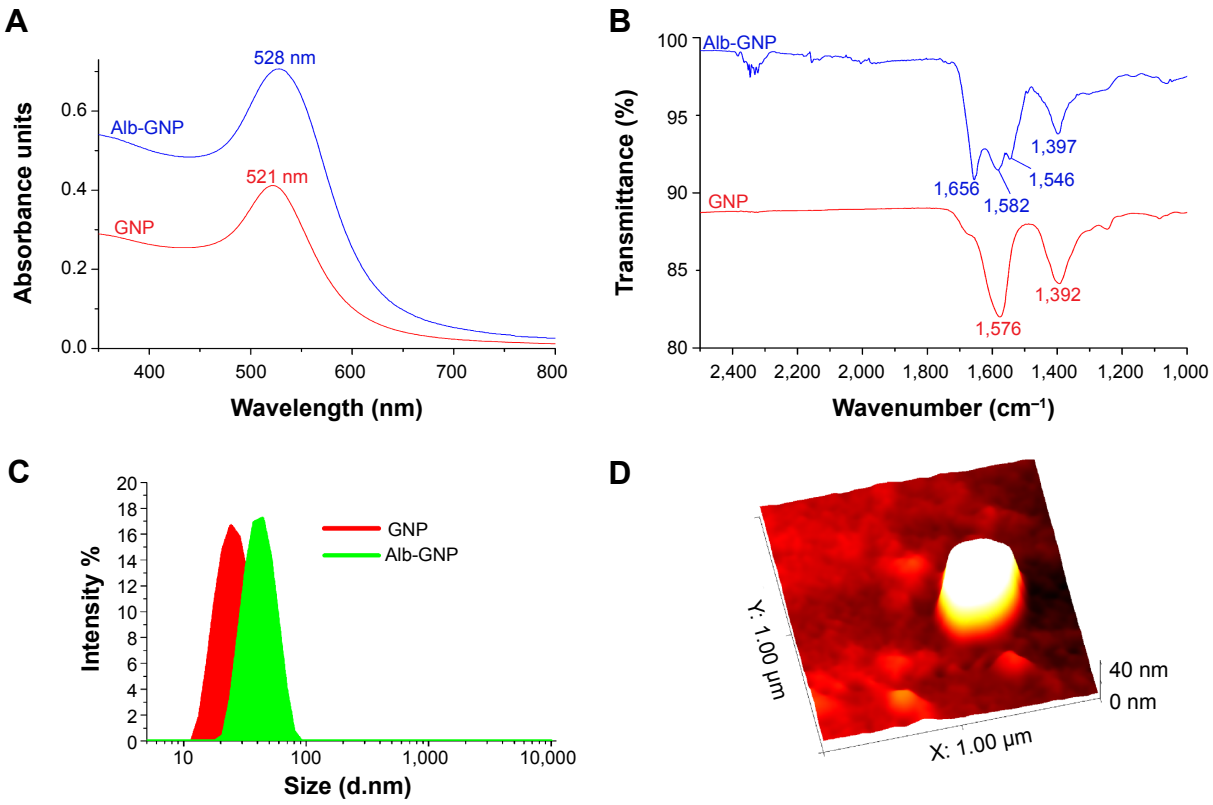

Figure 1 Characterization of GNP and Alb-GNPs.
Notes: (**A**) UV-Vis spectra of GNPs (red line) and BSA-GNP samples (blue line). (**B**) FT-IR spectra for GNP (red) and BSA-GNP (blue) in the 2,500–1,000 cm^{-1} region. (**C**) DLS size distribution curves for GNP (red) and BSA-GNP (green). (**D**) AFM image of a single BSA-GNP nanoparticle.
Abbreviations: GNP, gold nanoparticle; BSA, bovine serum albumin; IR, infrared; UV-Vis, ultraviolet visible; DLS, dynamic light scattering; AFM, atomic force microscopy.

1,582 cm^{-1}, respectively. Figure 1B clearly indicates that the citrate ions from the GNPs surface were replaced by BSA during the functionalization step of the GNPs. This phenomenon can be explained by the fact that BSA has a tertiary structure stabilized by 17 internal disulfide bonds between 34 cysteine residues, which accounts for the higher affinity of the protein for GNPs, compared with that of citrate ions.[18]

The size of the GNPs before and after functionalization with the serum Alb was also measured by the dynamic light scattering technique. A size distribution curve for both GNP and Alb-GNP is shown in Figure 1C; both samples were monodispersed and presented good stability at room temperature and at 37°C. The increase in size suggested by the red shift of the SPR peak of colloidal gold after functionalization is also confirmed by the DLS measurements. Citrate-capped GNPs had a mean diameter of 15 nm, while Alb-GNP had a mean diameter of 49 nm.

AFM measurements were conducted on the Alb-GNP sample to further investigate the size and shape of the obtained nanoparticles. Figure 1D shows an image of Alb-GNP; in this case, spherical nanoparticles with an average diameter of ~41 nm can be observed. The average diameter for the Alb-GNP determined by DLS was approximately 49 nm. This can be explained by the fact that the DLS technique provides a mean hydrodynamic diameter of GNPs surrounded by the Alb molecules and the solvation layers.[19] In addition, a PDI (polydispersity index) of 0.464 was obtained for GNP, while for Alb-GNP the resulting PDI was 0.549.

The mechanism of selective internalization of Alb-GNPs inside the malignant liver cells

In order to shed light on the molecular mechanisms involved in the specific uptake of Alb-GNPs in HepG2 cells, we investigated the possibility that a 60 kDa glycoprotein, Gp60, which is known to function in Alb transcytosis in malignant cells, was involved in the selective uptake of Alb bound to GNPs. To accomplish this, we allowed the 50 μg/mL Alb-GNP treated cells (1 hour) to incorporate Cy3–anti-Gp60 Ab for 30 minutes at 37°C. To that end, we obtained fluorescent images demonstrating the activation of the Gp60 receptors as suggested by Cy3 fluorescence (Figure 2B).

We next assessed the affinity of Alb-GNPs nano-biosystem for liver cancer cells using dark-field microscopy imaging. As seen in Figure 2A, the incorporation of GNPs by HepG2 cells was significantly higher in liver cancer cells with punctuate, refringent nanostructures spread all over the cytoplasm with red fluorescence colocalization, strongly suggesting selective targeting of the Cy3 marked receptors (Figure 2). For control cells, a weaker activation of Gp60 receptors was noticed, an observation that was confirmed by dark-field microscopy (Figure 2).

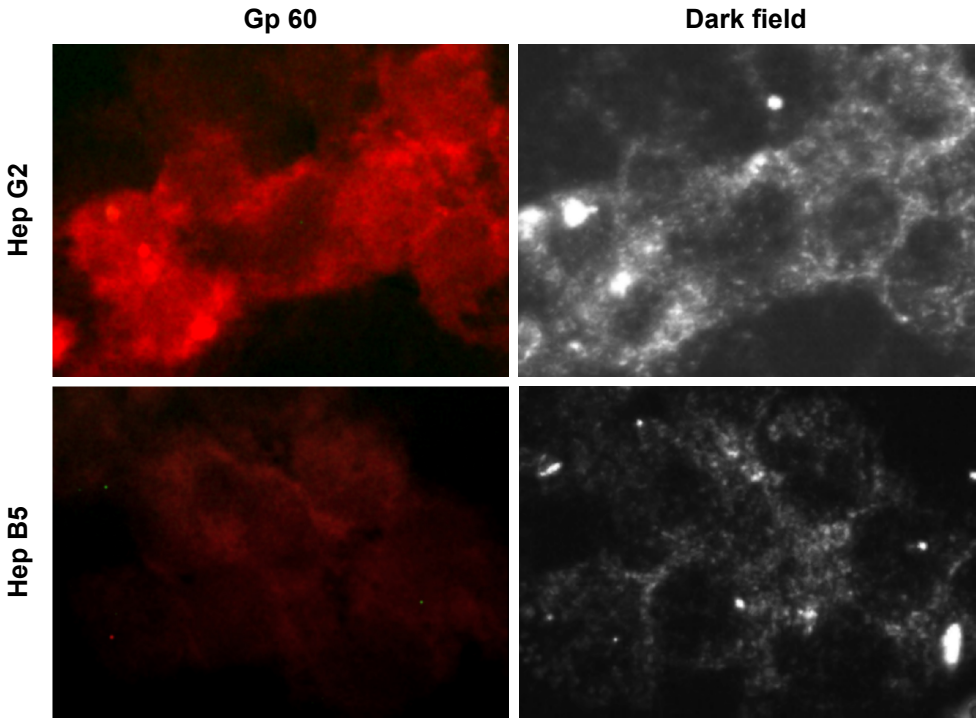

Figure 2 GNPs albumin-mediated in vitro endocytosis mechanism in human liver cancer cells.
Notes: Exposure to 50 μg/mL Alb-GNPs for 1 hour, 37°C. Dark field light microscopy images of Alb-GNPs uptake into Hep G2 cells or Hep B5 cells (control). Magnification: 80×.
Abbreviations: AU, absorbance units; Alb-GNPs, albumin-conjugated gold nanoparticles.

Alb-GNPs photothermal treatment causes severe ER and GA morphologic changes in HepG2 cells but not in HepB5

The ER is an architecturally complex membrane system of folded sacs responsible for protein production and folding, lipid synthesis, translocation and post-translation modification. Various stress stimuli such as radiation, drugs, thermal damage, or chemical agents cause ER stress with subsequent accumulation of unfolded or misfolded proteins in the ER that further generate nutrient deprivation, metabolic disturbances, intraluminal calcium depletion, oxidative stress, and DNA damage. To survive, these cells under stress must develop various mechanisms in ER function and ER stress. If unresolved, ER stress may trigger cell death by induction of apoptosis.[20]

Research data suggest that programmed cell death mechanisms believed to induce apoptosis occur by two major mechanisms – the intrinsic pathway, mainly controlled at the level of the mitochondria, and the extrinsic pathway, regulated by the binding of specific death ligands to their receptors on the cell surface.[21] Recently, it was found that other sites of the malignant cell organelles such as the ER and the GA can trigger programmed cell death cascades, causing a general dysfunction and cellular death.[20]

As seen in Figure 3, we observed that photothermal (PT) treatment mediated by Alb-GNPs causes a collapse of the GA. The disruptive effect on the GA ultimately leads to malfunction of ER in HepG2 cells. To analyze this hypothesis, cells were treated at various concentrations and various incubation times, and further stained specifically for analysis of changes in ER morphology by fluorescence microscopy. As shown in Figure 3, PT treatment caused a severe, concentration-dependent dilation of ER membranes. ImageJ quantification of fluorescent areas revealed a significant decrease ($P<0.005$) in both red and green fluorescence following Alb-GNPs mediated PT treatment in HepG2 cells, but not in control HepB5 cells. This dramatic change in ER morphology occurred prior to the onset of appreciable apoptosis and did not occur in HepB5-treated cells, strongly suggesting that these effects were specific to cancer liver treatment and not a general feature of any type of cell. Taken together, these data suggest that HepG2 cells may be intrinsically sensitive to this particular type of GNP-mediated thermal ablation.

Annexin-V Cy3 Apoptosis Detection Kit

To assess the apoptotic effect of Alb-GNPs and laser treatment, we examined the translocation of PS groups from the inner to the exterior surface of the liver cancer cells membrane as a marker of early apoptosis state induction. Using the high affinity of annexin for PS groups, we were able to detect the apoptosis rate in all samples. Our results (Figure 4) show a

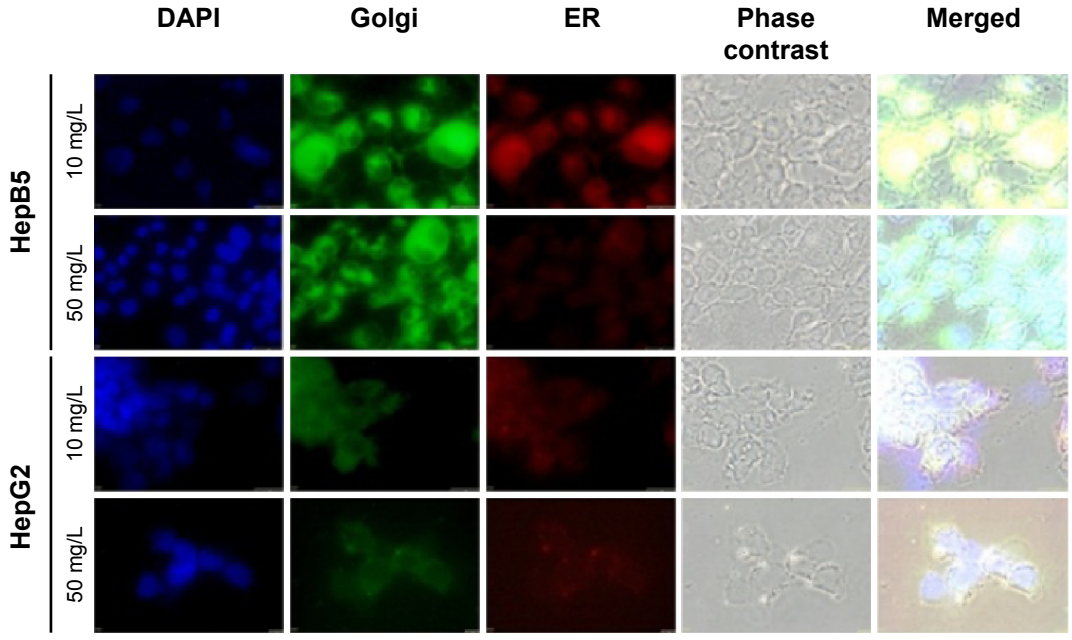

Figure 3 The concomitent detection of Golgi apparatus and ER function following Alb-GNPs mediated photothermal treatment.
Notes: Exposure to 10 μg/mL Alb-GNPs (1 hour, 37°C), followed by laser excitation (3 minutes, 808 nm, 2W/cm^2). Upper row: HepB5 cells: normal red and green fluorescence is visible, suggesting that HepB5 cells function normally. Third row: HepG2 cells: red and green fluorescence is less visible, with mild architectural changes in both ER and Golgi. Second row: exposure to 50 μg/mL Alb-GNPs (1 hour, 37°C), followed by laser excitation (3 minutes, 808 nm, 2W/cm^2). Bottom row: HepB5 cells: normal green fluorescence suggest a normal function of the GA, with mild disturbance of ER function. HepG2 cells: red and green fluorescence is less visible, with severe architectural changes in both ER and GA suggesting lack of function in these organelles. Magnification: 60×.
Abbreviations: ER, endoplasmic reticulum; GA, Golgi apparatus; Alb-GNPs, albumin-conjugated gold nanoparticles.

higher proapoptotic effect in the treated samples as compared with the control. Increasing effects were obtained for treatment with the increase of Alb-GNPs solutions' concentration (5, 10, 50 μg/mL). The highest red staining intensity and presence (generated by Cy3 bound to annexin V) has been observed in the samples treated with 50 μg/mL Alb-GNPs followed by laser irradiation. ImageJ quantification of all fluorescent images following laser-mediated treatment with Alb-GNPs (with concentrations above 10 μg/mL) revealed a significantly increased red fluorescence compared with control, suggesting strong induction of apoptosis (chi square, $P<0.05$).

Alb-GNPs PT treatment causes GA dysfunction with consequent caspase-3 pathway activation

As seen in Figure 5, we showed that PT ablation of Alb-GNPs causes a collapse of the GA. The ability of Alb-GNPs' PT treatment to cause direct Golgi stress prompted us to next investigate the effects of this therapeutic method on caspase-3 pathway in malignant HepG2 cells. We first used fluorescence microscopy to display the cellular distribution of caspase-3 in HepG2 cells with or without Alb-GNPs treatment. In accordance with earlier reports in other malignant cells, the immunostaining pattern of caspase-3 was represented by punctuate structures homogenously localized in the cytoplasmic region. Following 1 hour of PT treatment with 50 μg/mL Alb-GNPs, caspase-3 lost its normal cellular localization pattern and appeared throughout the nucleus. The GA in these cells could no longer be visualized by the Golgi staining, strongly suggesting the collapse of this structure. Several reports have described a particular apoptotic pathway in malignant cells triggered by ER/Golgi stress and that further induces the mitochondrial cell death cascade.

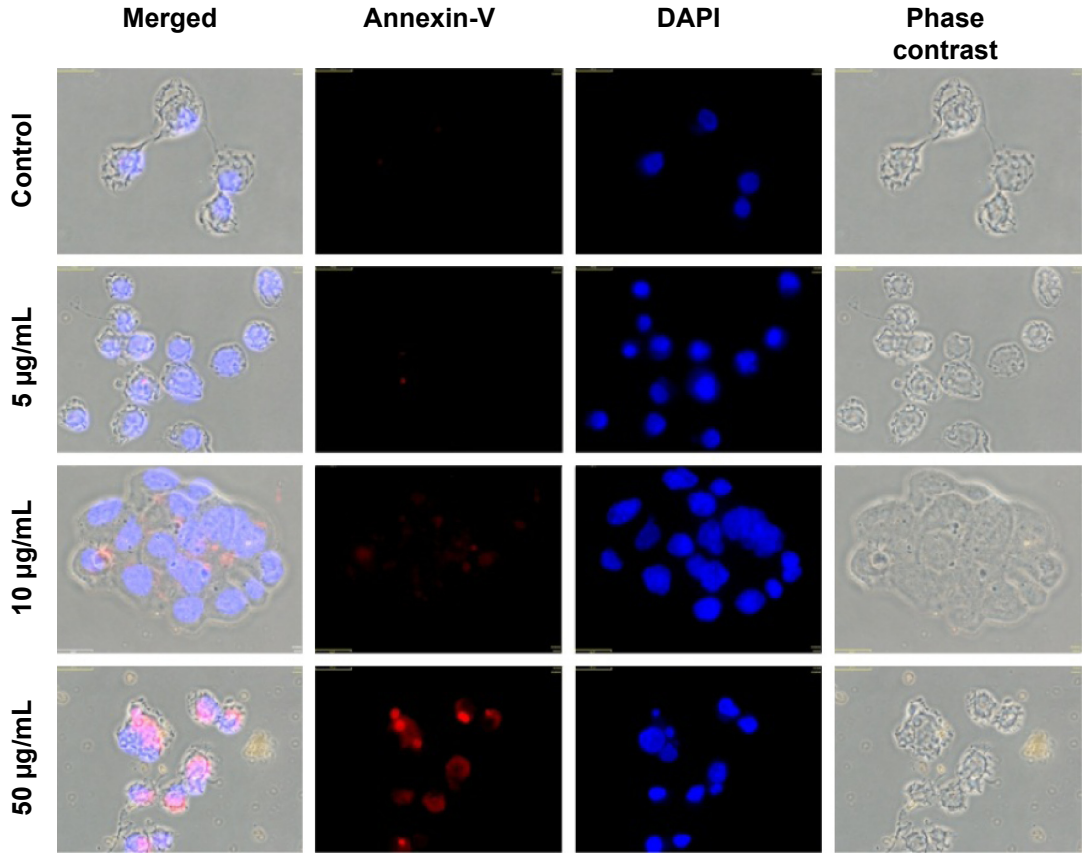

Figure 4 Detection of apoptosis using Annexin V-cy3.

Notes: Control sample followed standard cell culture conditions. Test cells were treated with Alb-GNPs with different concentrations 5, 10, and 50 μg/mL, respectively and laser irradiated. Consequently, all samples were stained with annexin-cy3 for 5 minutes (RT, dark). Nucleus staining was also performed using DAPI blue-fluorescence. Control sample (no Alb-GNPs exposure, no irradiation). No red fluorescence was observed. Exposure to 5 μg/mL Alb-GNPs (1 hour, 37°C), followed by laser excitation (3 minutes, 808 nm, 2W/cm^2). Red fluorescence is displayed in a reduced number of cells, granular aspect coming from limited number of PS groups exposed on the outer surface of the membrane. Exposure to 10 μg/mL Alb-GNPs (1 hour, 37°C), followed by laser excitation (3 minutes, 808 nm, 2W/cm^2), increased the number of early-apoptosis entrance cells. Red fluorescence aspect is diffuse, suggesting intense PS translocation process. Exposure to 50μg/mL Alb-GNPs (1 hour, 37°C), followed by laser excitation (3 minutes, 808 nm, 2W/cm^2). The majority of cells present intense, diffuse, red Cy3 fluorescence covering the entire outer surface of the membrane suggesting a highly intense pro-apoptotic effect. Magnification: 60×.

Abbreviations: GNPs, gold nanoparticles; RT, room temperature; DAPI, 4',6-diamidino-2-phenylindole; PS, phosphatidylserine; Alb, albumin.

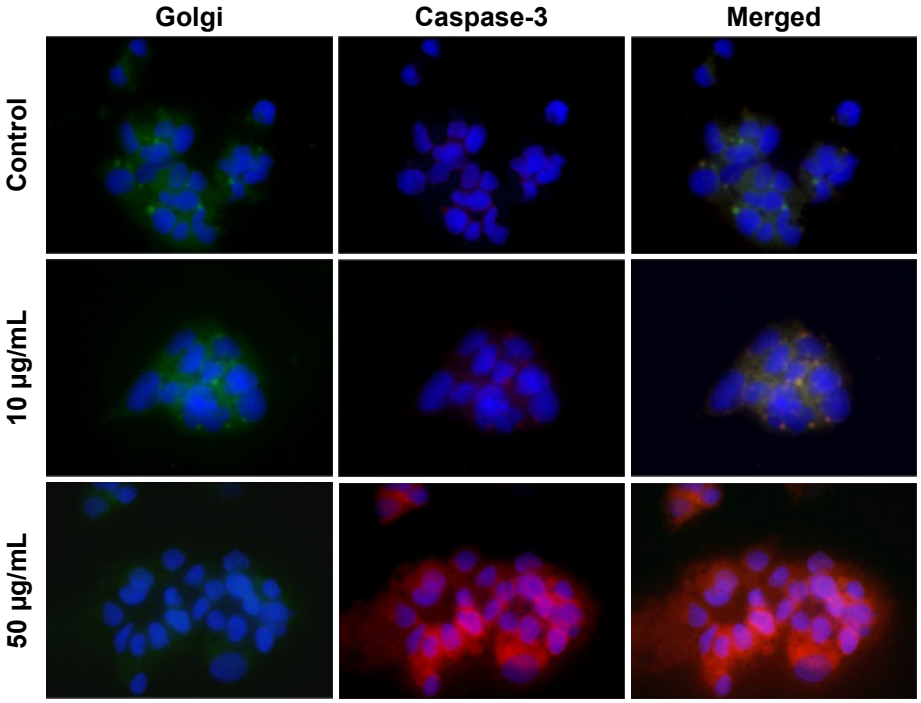

Figure 5 The concomitent detection of Golgi apparatus function and caspase 3 pathway.
Notes: Upper row: control sample (no Alb-GNPs exposure: low red fluorescence is visible, suggesting that Hep G2 cells have low apoptotic state under normal conditions; in contrast Golgi function is normal as suggested by green fluorescence. Middle row: exposure to 10 μg/mL Alb-GNPs (1 hour, 37°C), followed by laser excitation (3 minutes, 808 nm, 2W/cm^2). Lower green fluorescence intensity staining combined with increased red fluorescence suggest low Golgi function with moderate activation of caspase 3 pathway. Bottom row: exposure to 50 μg/mL Alb-GNPs (1 hour, 37°C), followed by laser excitation (3 minutes, 808 nm, 2W/cm^2). The majority of cells present intense, inhomogenuous, granular aspect of red fluorescence with lack of fluorescence staining suggesting an intense activation of caspase 3 apoptotic pathway. Magnification: 60×.
Abbreviation: Alb-GNPs, albumin-conjugated gold nanoparticles.

Assessment of cellular toxicity following Alb-GNPs administration

Before testing the in vitro response of Alb-GNPs-treated cells to laser irradiation, we investigated the possible effect of in vitro cytotoxicity induced by the administration of the developed nano-biosystems. HepG2 cells and the epithelial cells were treated with various concentrations of Alb-GNPs at various incubation periods. Flow cytometry combined with annexin staining was used to assess the cytotoxic effect of Alb-GNPs administration.

As seen in Figure 6, after 1 hour of incubation, HepG2 exposed to 50 μg/mL of Alb-GNPs showed a 1.9% decrease in viability, compared with 2.3% for GNPs ($P>0.05$). For human hepatocytes exposed to 50 μg/mL of Alb-GNPs, the decrease in viability was 1.6%, compared with the GNPs-only treated sample, where the percentage of viable cells was 97.1%. The statistical data showed that nanomaterial exposure per se induced no significant cytotoxic effects, and appears to be safe for administration in biological systems.

The next step in order to eliminate any potential errors was represented by a 2-minute irradiation of a sample of cells without nanoparticles, using an 808 nm and 2 W laser beam. There were no signs of cellular death among the cells after irradiation. The process demonstrates the transparency of HepG2 for NIR beam.

Assessment of cellular necrosis after laser treatment and Alb-GNPs administration

The postirradiation apoptotic rate of HepG2 cells treated with Alb-GNPs ranged from 25.8% (for 5 μg/mL) to 48.2% (for 50 μg/mL) at 60 seconds, while at 30 minutes the necrotic rate increased from 35.7% (5 μg/mL) to 52.3% (50 μg/mL), P-value <0.001. Significantly lower necrotic rates were obtained in irradiated HepB5 cells treated for 60 seconds and 30 minutes at concentrations ranging from 5 to 50 μg/mL (8.3%–24.3% for 60 seconds, 14.7%–22% for 30 minutes). As displayed in Figure 6, the optimal apoptotic effect of malignant cells after incubation with Alb-GNPs was obtained at a concentration of 5 μg/mL and a 60-second exposure (HepG2/HepB5: 48.2%/24.3%). Following 60 minutes of incubation time, the difference among apoptotic rates was also statistically significant among the two cell lines for low/medium concentrations of Alb-GNPs (48.3% – 5 μg/mL, 57.9% – 10 μg/mL, 70% – 50 μg/mL for HepG2; 19.2%–5 μg/mL, 22.1%–10 μg/mL, 34.1%–50 μg/mL

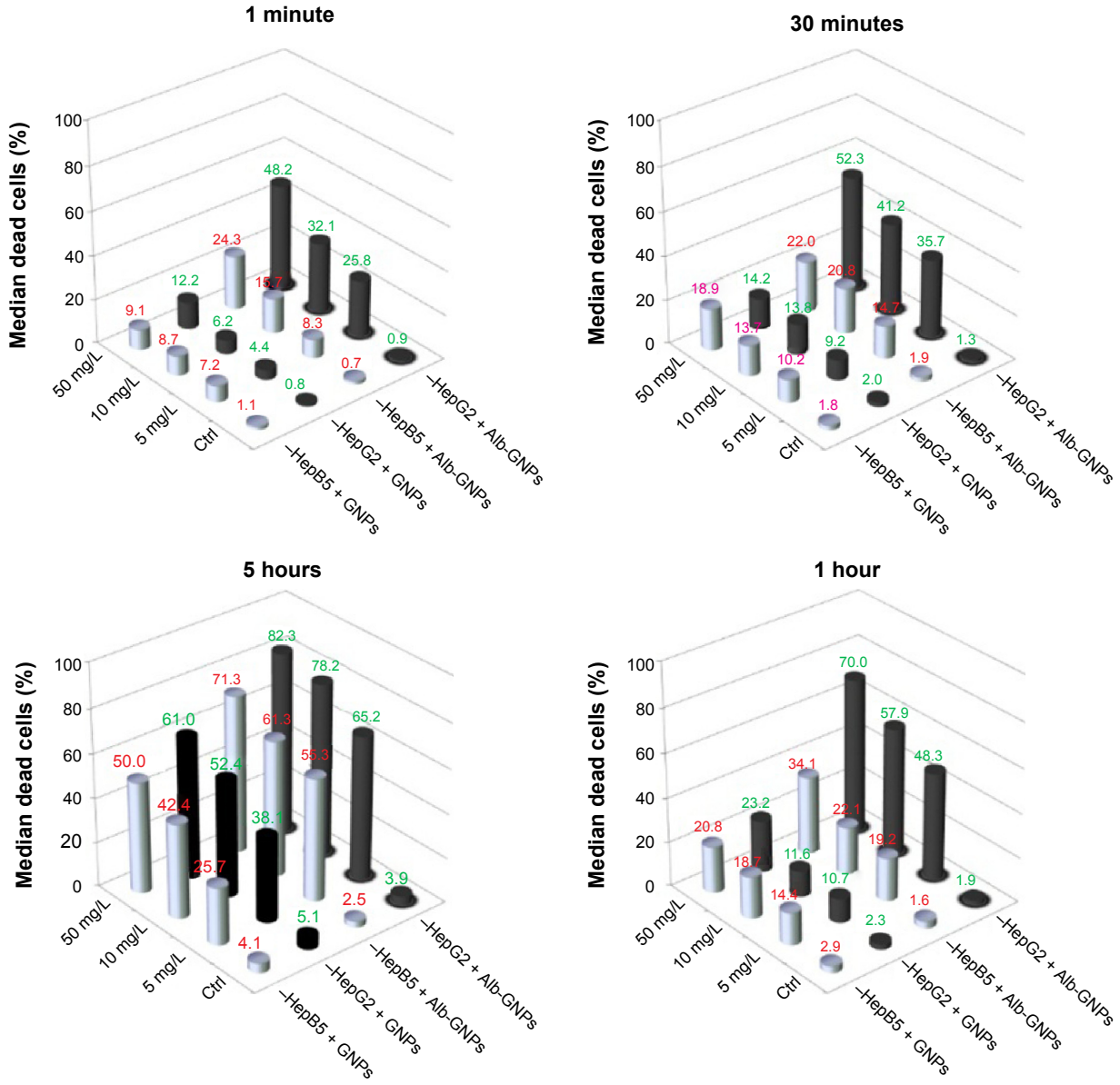

Figure 6 Cytotoxicity and photothermal activity in liver cancer cells and HepB5 cells following treatment with Alb-GNPs.
Notes: The results represent quantification by flow cytometry (%) of Annexin-Cy5 positive cells after photothermal treatment as described.
Abbreviations: Ctrl, control; Alb-GNPs, albumin-conjugated gold nanoparticles.

for HepB5). *P*-values were <0.003 for all comparisons between nanomaterial.

After 5 hours of incubation, a significant apoptotic rate between the two cell lines recorded a nonsignificant difference between the apoptotic effect of the two types of cells ($P>0.05$).

Discussion

The main goal of this investigation was to develop and test a novel method of treatment for human HC. Preliminary data from the literature supports the involvement of Alb in tumor growth. The implication is that Alb enhances the tumor expansion since it is used for the synthesis of various cellular compartments.[22,23]

To investigate the toxicity effects of the nanoconjugates, HepG2 and HepB5 in culture medium were exposed and incubated with Alb-GNPs at various concentrations and incubation times. Consistent with other scientific reports, we showed that even high concentrations of GNPs bioconjugate do not exhibit cytotoxic effects. Nevertheless, toxicity, a major obstacle for the successful use of GNPs in clinical applications, may be minimized by the administration of reduced nanoconjugates or by biofunctionalization with biologic moieties.

Further, we used Alb-GNPs as heat-inducing agents under the laser radiation during the nanophotothermolysis process. This method is based on the presence and clustering of Alb-GNPs inside the cells and their highly optical absorption capabilities,[24] responsible for inducing thermal effects, especially under NIR irradiation where the biological systems have low absorption and a high transparency.[25] The optoelectronic transitions onto the external surface of the GNPs clusters generate thermal energy that rapidly diffuses into the subcellular compartments where the nanoconjugates are present.[26]

Using a continuous laser irradiation, we obtained significant differences in HepG2 cells postirradiation apoptotic percentage ($P<0.05$) for concentrations of less than 20 μg/mL, at 60 seconds and 30 minutes of incubation between Alb-GNPs and GNPs. This finding may be particularly relevant under conditions where Alb-GNPs are present at low concentrations (eg, plasma levels after in vivo administration). To our knowledge, this is the first demonstration of impressive laser thermal ablation of liver cancer cells using Alb-GNPs.

In the present study, we observed that treating HepG2 with high concentrations of Alb-GNPs for 5 hours, the percentage of dead HepG2 cells is not significantly different from that of epithelial cells. This finding suggests a nonselective, passive intracellular diffusion of nanomaterial inside cells when cells are exposed to high concentrations of nanomaterials for longer periods of time, as suggested by other authors.[27]

In contrast, for incubation times lower than 30 minutes, we obtained a selective necrosis of HepG2 cells treated with Alb-GNPs, independent of the concentration. In cellular systems, the molecular membrane association/dissociation processes are of very short terms, ranging from seconds to minutes.[28] Therefore, our finding could be of decisive importance when using Alb-GNPs for the in vivo targeting of liver cancer applications.

Alb-GNPs-mediated PT ablation generates a selective apoptosis in HepG2 cells through activation of the caspase-3 pathway. As a result of laser irradiation, caspase-3 appears to function as a trigger caspase, and we have proved that apoptosis is initiated at the GA. We next showed that following Alb-GNPs laser-mediated treatment, caspase-3 can translocate to cytoplasm. Our observation is also suggested by several authors, showing that mutation of the caspase cleavage sites of the caspase-3 substrate golgin-160 decreases the sensitivity to cytostatic drugs as well as other anticancer agents.[29] The presented results suggest that caspase-3 plays an important role in the initiation of Alb-GNPs laser-induced apoptosis, and highlights a potential link between the Golgi and death receptor apoptotic cascades in PT treatment using GNPs bound to specific antibodies.

In response to the strong demand for the development of specific and site-sensitive anticancer therapies, novel pathways, involving GA, and programmed apoptosis are all being recognized as potential drug targets.[30,31]

Research data have shown that when apoptosis occurs in malignant cells, GA is being disassembled in a manner similar to that which occurs in mitosis, a process that is mediated by Polo-like kinase-3 (Plk3) that also plays a crucial role in the DNA damage checkpoints activation.[32]

On the other hand, a pool of death receptors that populate the GA in eukaryotic cells may also be responsible for the initiation of cellular apoptosis.[33]

Because the Golgi system plays an important role in the induction of apoptosis, triggering it holds great hopes in the development of novel anticancer therapies.[34] Therefore, our results could be of decisive importance for the development of novel nanomediate thermal therapies against liver cancer.

These results may represent a first step in the process of a novel in vivo treatment method of liver cancer cells using nanolocalized thermal ablation by laser heating.

Conclusion

Considering all these data, we may assert that administration of Alb-functionalized GNPs leads to increased intracellular uptake in liver cancer cells by selective targeting of Gp60 receptors located on the cellular membrane. We have shown that following laser irradiation, photoexcitation of GNPs exhibits increased apoptotic events initiated by GA–ER disintegration with further activation of caspase-3 apoptotic caspase.

These results may represent a first step in the process of a novel in vivo treatment method of liver cancer cells using nanolocalized thermal ablation by laser heating. From a surgical point of view, the ultrasound identification of the tumor and its vascular supply, the intra-arterial administration of the functionalized GNPs, as well as the external laser irradiation, could all be safely achieved in patients by means of minimally invasive surgery, with major benefits for the patient (eg, laparoscopic approach or percutaneous approach under ultrasound/CT guidance).

However, further research is required to fully understand the mechanisms of selective binding of Alb-GNPs on HepG2 cells. In addition, further research is required for a careful assessment of unexpected toxicities and biological interactions of Alb-GNPs when administered on living organisms.

Acknowledgments

This paper was published under the aegis of the European Social Fund, Human Resources Development Operational

Programme 2007–2013, project number POSDRU/159/1.5/S/138776. We specifically wish to acknowledge grant numbers PN-II-PT-PCCA-2011-3.1-1586, PN-II-PT-PCCA-2011-3.1-1551, PN-II-PT-PCCA-2011-3.2-1289, PN-11-PT-PCCA-2013-4-1553, and PN-II-ID-PCE-2012-4-0243.

Disclosure

The authors report no conflicts of interest in this work.

References

1. Jemal A, Bray F, Center MM, Ferlay J, Ward E, Forman D. Global cancer statistics. *CA Cancer J Clin*. 2011;61(2):69–90.
2. Blachier M, Leleu H, Peck-Radosavljevic M, Valla D, Roudot-Thoraval F. The burden of liver disease in Europe: a review of available epidemiological data. *J Hepatol*. 2013;58(3):593–608.
3. Conde J, Doria G, Baptista P. Noble metal nanoparticles applications in cancer. *J Drug Deliv*. 2012;2012:751075.
4. Mocan L, Ilie I, Tabaran FA, et al. Surface plasmon resonance-induced photoactivation of gold nanoparticles as mitochondria-targeted therapeutic agents for pancreatic cancer. *Expert Opin Ther Targets*. 2013;17(12):1383–1393.
5. Yang M, Jiang X, Liang L, Yang J. Application of nanobiotechnology in cancer: creation of nanooncology and revolution in cancer research and practice. *World J Cancer Res*. 2013;1(1):24–36.
6. Akhter S, Ahmad MZ, Ahmad FJ, Storm G, Kok RJ. Gold nanoparticles in theranostic oncology: current state-of-the-art. *Expert Opin Drug Deliv*. 2012;9(10):1225–1243.
7. Dreaden EC, Austin LA, Mackey MA, El-Sayed MA. Size matters: gold nanoparticles in targeted cancer drug delivery. *Ther Deliv*. 2012;3(4):457–478.
8. Brannon-Peppas L, Blanchette JO. Nanoparticle and targeted systems for cancer therapy. *Adv Drug Deliv Rev*. 2012;64:206–212.
9. Nanda R, Chennamaneni P, Gibson J, et al. Abstract P2-16-21: a randomized phase I trial of nanoparticle albumin bound paclitaxel (nab-paclitaxel, Abraxane®) with or without mifepristone for advanced breast cancer. *Cancer Res*. 2013;73(24 Suppl):P2-16-21–P2-16-21.
10. Jain S, Hirst D, O'sullivan J. Gold nanoparticles as novel agents for cancer therapy. *Br J Radiol*. 2014;85(1010):101–113.
11. Gupta S, Stafford RJ, Javadi S, et al. Effects of near-infrared laser irradiation of biodegradable microspheres containing hollow gold nanospheres and paclitaxel administered intraarterially in a rabbit liver tumor model. *J Vasc Interv Radiol*. 2012;23(4):553–561.
12. Iancu C, Mocan L, Bele C, et al. Enhanced laser thermal ablation for the *in vitro* treatment of liver cancer by specific delivery of multiwalled carbon nanotubes functionalized with human serum albumin. *Int J Nanomedicine*. 2011;6:129.
13. Stehle G, Wunder A, Sinn H, et al. Pharmacokinetics of methotrexate-albumin conjugates in tumor-bearing rats. *Anticancer Drugs*. 1997;8(9):835–844.
14. Hartig SM. Basic image analysis and manipulation in ImageJ. *Curr Protoc Mol Biol*. 2013: Unit 14.15.
15. Shang L, Wang Y, Jiang J, Dong S. pH-dependent protein conformational changes in albumin: gold nanoparticle bioconjugates: a spectroscopic study. *Langmuir*. 2007;23(5):2714–2721.
16. Singh S, Kaur R, Chahal J, Devi P, Jain D, Singla M. Conjugation of nano and quantum materials with bovine serum albumin (BSA) to study their biological potential. *J Lumin*. 2013;141:53–59.
17. Wang Y, Ni Y. Combination of UV–vis spectroscopy and chemometrics to understand protein–nanomaterial conjugate: a case study on human serum albumin and gold nanoparticles. *Talanta*. 2014;119:320–330.
18. Park J, Shumaker-Parry JS. Structural study of citrate layers on gold nanoparticles: role of intermolecular interactions in stabilizing nanoparticles. *J Am Chem Soc*. 2014;136(5):1907–1921.
19. Mandal G, Bardhan M, Ganguly T. Interaction of bovine serum albumin and albumin-gold nanoconjugates with l-aspartic acid. A spectroscopic approach. *Colloids Surf B Biointerfaces*. 2010;81(1):178–184.
20. Tabas I, Ron D. Integrating the mechanisms of apoptosis induced by endoplasmic reticulum stress. *Nat Cell Biol*. 2011;13(3):184–190.
21. Boelens J, Lust S, Offner F, Bracke ME, Vanhoecke BW. Review. The endoplasmic reticulum: a target for new anticancer drugs. *In Vivo*. 2007;21(2):215–226.
22. Tiruppathi C, Song W, Bergenfeldt M, Sass P, Malik AB. Gp60 activation mediates albumin transcytosis in endothelial cells by tyrosine kinase-dependent pathway. *J Biol Chem*. 1997;272(41):25968–25975.
23. Schilling U, Friedrich EA, Sinn H, Schrenk HH, Clorius JH, Maier-Borst W. Design of compounds having enhanced tumour uptake, using serum albumin as a carrier – part II. In vivo studies. *Int J Rad Appl Instrum B*. 1992;19(6):685–695.
24. Honda M, Saito Y, Smith NI, Fujita K, Kawata S. Nanoscale heating of laser irradiated single gold nanoparticles in liquid. *Opt Express*. 2011;19(13):12375–12383.
25. Huo S, Ma H, Huang K, et al. Superior penetration and retention behavior of 50 nm gold nanoparticles in tumors. *Cancer Res*. 2013;73(1):319–330.
26. Kim D, Jon S. Gold nanoparticles in image-guided cancer therapy. *Inorg Chim Acta*. 2012;393:154–164.
27. Pokharkar V, Bhumkar D, Suresh K, Shinde Y, Gairola S, Jadhav S. Gold nanoparticles as a potential carrier for transmucosal vaccine delivery. *J Biomed Nanotechnol*. 2011;7(1):57–59.
28. Fesce R, Meldolesi J. Peeping at the vesicle kiss. *Nat Cell Biol*. 1999;1(1):E3–E4.
29. Mahmood M, Karmakar A, Fejleh A, et al. Synergistic enhancement of cancer therapy using a combination of carbon nanotubes and anti-tumor drug. *Nanomedicine (Lond)*. 2009;4(8):883–893.
30. Van den Elsen JM, Kuntz DA, Rose DR. Structure of Golgi α-mannosidase II: a target for inhibition of growth and metastasis of cancer cells. *EMBO J*. 2001;20(12):3008–3017.
31. Cheng Y, Samia AC, Meyers JD, Panagopoulos I, Fei B, Burda C. Highly efficient drug delivery with gold nanoparticle vectors for in vivo photodynamic therapy of cancer. *J Am Chem Soc*. 2008;130(32):10643–10647.
32. Lopez-Sanchez I, Sanz-Garcia M, Lazo PA. Plk3 interacts with and specifically phosphorylates VRK1 in Ser342, a downstream target in a pathway that induces Golgi fragmentation. *Mol Cell Biol*. 2009;29(5):1189–1201.
33. Wouters BG, Koritzinsky M. Hypoxia signalling through mTOR and the unfolded protein response in cancer. *Nat Rev Cancer*. 2008;8(11):851–864.
34. Taylor RC, Cullen SP, Martin SJ. Apoptosis: controlled demolition at the cellular level. *Nat Rev Mol Cell Biol*. 2008;9(3):231–241.